Combining hillslope erosion and river connectivity models to assess large scale fine sediment transfers: Application over the Rhône River (France)

Clément Fabre, Mathieu Fressard, Simone Bizzi, Flora Branger, Hervé Piegay

Combining hillslope erosion and river connectivity models to assess large scale fine sediment transfers: application over the Rhône River (France).

Clément Fabre[1,*], Mathieu Fressard[1,4], Simone Bizzi[2], Flora Branger[3],Hervé Piegay[1]

[1]Univ. Lyon, University Lumière Lyon 2, UMR 5600 CNRS-Environnement Ville Société – LYON, F-69007, France.

[2] Department of Geosciences, University of Padova, 35122 Padua, Italy

[3] INRAE, UR RiverLy, Centre de Lyon-Grenoble, Villeurbanne, France

[4]Normandie Univ., University of Caen Normandie, UMR 6266 CNRS-Identité et Différenciation de l'Espace, de l'Environnement et des Sociétés – CAEN, F-14000, France

Abstract:

Sediment connectivity at the catchment scale includes the processes linking sediment sources, sinks and the river outlet. Soil erosion models usually estimate yields without considering riverine processes or human infrastructures that may affect sediment connectivity. Quantifying these processes at a large scale is determinant to understanding sediment transfers from the continental lands to the marine ecosystems. This study tries to fill this gap by coupling the soil erosion model WaTEM/SEDEM (WS) with the riverine connectivity tool CASCADE to quantify sediment fluxes in the Rhône watershed. The coupling returned a good fitting with deviations of -51.7%. WS alone predict better the exported fluxes with a deviation of -34.9%. Nevertheless, this paper shows the importance of considering connectivity and transport capacity to develop a more realistic representation of fine sediment dynamics at large scale. However, connectivity tools depend on the quality of the models (soil erosion and

hydrology) and the geomorphological data on which they depend, which is a limiting factor in large-scale studies.

Keywords: sediment connectivity; soil erosion models; suspended load; Rhône

1 Introduction

Rivers are more than pipes transporting water. They play a significant role in carrying sediments and depositing them downstream or into oceans (Zarfl and Dunn, 2022). These transported materials shape river morphology and riverine ecosystems by conveying nutrients and pollutants. Modifications in sediment fluxes and connectivity have huge impacts on the stability of river systems and the biodiversity or the socioeconomic activities that rely on them (Downs and Piegay, 2019; Kondolf et al., 2018; Zarfl and Dunn, 2022).

Anthropogenic disturbances on rivers, such as dams or intensive agriculture, impact sediment supply and consequently lead to significant river-process shifts (Kondolf et al., 2014; Richter et al., 2010; Vörösmarty et al., 2003). In addition, developing multiple dams creates a trapping effect that may induce sediment starvation downstream. In this sense, the global fluvial suspended load decreased by 50% between 1950 and 2010 (Syvitski et al., 2022). Moreover, Kondolf (1997) showed that the large amounts of clear water delivered by dams affect the geomorphology of riverbeds downstream, leading to ecosystem degradation. River mouths are also threatened by this decrease in sediment delivery due to coastal degradation and the shrinking of the river delta (Kondolf et al., 2018; 2022; Syvitski et al., 2009).

The concept of sediment connectivity has been used for decades to describe the source-to-sink sediment transport dynamics (Heckmann et al., 2018; Najafi et al., 2021). It can be defined as “the degree to which a catchment facilitates the transfer of water and sediment through itself, through coupling relationships between its components; it reflects the (dis-)continuity of runoff and sediment pathways at a given point in time” (Heckmann et al., 2018). It has proven helpful in characterising sediment distribution patterns (spatial and temporal), sediment cascades, and channel aggradation and degradation processes (Borrelli et al., 2018; Brierley et al., 2022; Cavalli et al., 2013). Several authors state that the application of numerical models is necessary to develop and apply the concept (especially at a regional scale) since the diversity of the processes involved at multiple spatiotemporal scales limits the feasibility of empirical studies, as those in few occasions undertaken in small well-monitored catchments (e.g. Fryirs et al., 2007; Heckmann et al., 2018; Schmitt et al., 2016).

For the numerical modelling of sediment transport at the regional scale, the scientific community has developed two main types of models. The first class of models is soil erosion models, which represent the detachment of fine sediment based on empirical relationships mostly calibrated on soil particles affected by runoff processes depending on rainfall intensity and land use type). These approaches mainly rely on the Universal Soil Loss Equation (USLE) or its adaptations. They have been extensively applied to assess the erosion potential of hillslopes and their connectivity to the river network (Panagos et al., 2015). Applications of WaTEM/SEDEM (Borelli et al., 2018; Van Oost et al., 2000; Van Rompaey et al., 2001), INVEST (Hamel et al., 2017; Hooftman et al., 2023; Posner et al., 2016) are good examples of these attempts. These models almost completely neglect the complexity of geomorphic processes from different types of detachment processes and surface processes (e.g. landslides, runoff, and river processes) and consider rivers as pipes directly conveying sediments to the catchment outlets.

Another family of models focuses on sediment connectivity and tries to address the complexities of detachment and transport processes, but so far mostly focused on the semi-quantitative representation of landscape sediment connectivity (Cossart and Fressard, 2017; Fressard and Cossart, 2018; Heckmann et al., 2013; 2015). Recent efforts have been placed to simulate contemporary (or short-term) sediment connectivity and transport in the more realistic complexities of geomorphic surface processes occurring in a landscape (Baartman et al., 2018; Bizzi et al., 2021; Czuba and Foufoula-Georgiou, 2015; Hirschberg et al., 2021; Khan et al., 2021; Rossi et al., 2017; Schmitt et al., 2018).

In this context, we aim to contribute to filling a specific research gap with this work: coupling a soil erosion model (European scale WaTEM/SEDEM model developed by Borelli et al., 2018) with a river network sediment connectivity model (the CASCADE model – Schmitt et al., 2016; Tangi et al., 2019). We conducted this research on the French part of the Rhône River as a large set of validation data (i.e. Suspended Particulate Matter -SPM- field monitoring) was made available in the framework of the *Rhône Sediment Observatory* ("Observatoire des Sédiments du Rhône" – OSR; http://graie.org/osr/) and the Arc-Isère observatory (Thollet et al., 2021).

First, we aimed to represent in a more realistic way how fine sediments are transported in the fluvial network once they have been produced/generated on slopes and floodplains by runoff processes by coupling the two model types. Both approaches will be compared and discussed. We developed a stepwise comparison approach with a progressive rise in the degree of complexity of the models to assess the benefits of this coupling. Second, we estimated hot spots of sediment transport and deposition in the catchment with multiple

anthropogenic pressures. Finally, we discussed the benefits of such a model coupling and the prospects of further research in this domain.

2 Study area and observed data used for validation

The Rhône River flows through ca. 800 km in Switzerland and the South-East of France between its source in the Alps and its outlet in the Mediterranean Sea (Figure 1). The Rhône watershed covers about 97,800 km^2. In this study, only the French part of the catchment is studied, as the Swiss and the French parts are considered disconnected by Lake Geneva.

The French part of the Rhône covers 87,444 km², about 90% of the total area of the catchment. It presents multiple human infrastructures with 22 hydroelectric dams on the main river course (Dugué et al., 2015) and numerous dams in the main tributaries. Only two main dams are considered in this study as they are known to interrupt sediment connectivity (Figure 1). The outlet is considered at the last main monitoring site (Beaucaire; station 25a on Figure 1), just upstream of the Rhône delta. The average discharge at this station is about 1,700 m^3 s^{-1}. The Rhône watershed presents a marked climatic and geological diversity. The section from Lake Geneva to the confluence with the Saône River in Lyon (called the “Upper Rhône”) has a hydrological regime mainly influenced by snow and glacier melting. In this part, a few tributaries flow to the Rhône River, including the Arve or the Ain. The Saône River, its largest tributary in terms of discharge, is characterised by an oceanic pluvial regime, resulting in the highest discharges occurring in winter. The Isère, the second main tributary, comes from the Alps with a strong slope gradient and a snow-melt regime (highest discharges in summer).

Mediterranean hydroclimatic conditions influence the other southern tributaries. On the right bank, the Ardèche or the Gardon show low average water discharges but short and violent flash-flood events in autumn and spring. On the left bank, the Durance River, combining a snow-melt regime and a Mediterranean influence, has less rapid flood events but delivers higher discharges. The Rhône River ends its course surrounding the Camargue delta and flows in the Mediterranean Sea.

Since 2009, SPM transport has been monitored at the outlet of the main tributaries of the Rhône River and along the mainstem within the OSR framework. The locations of the monitoring sites are shown in Figure 1.

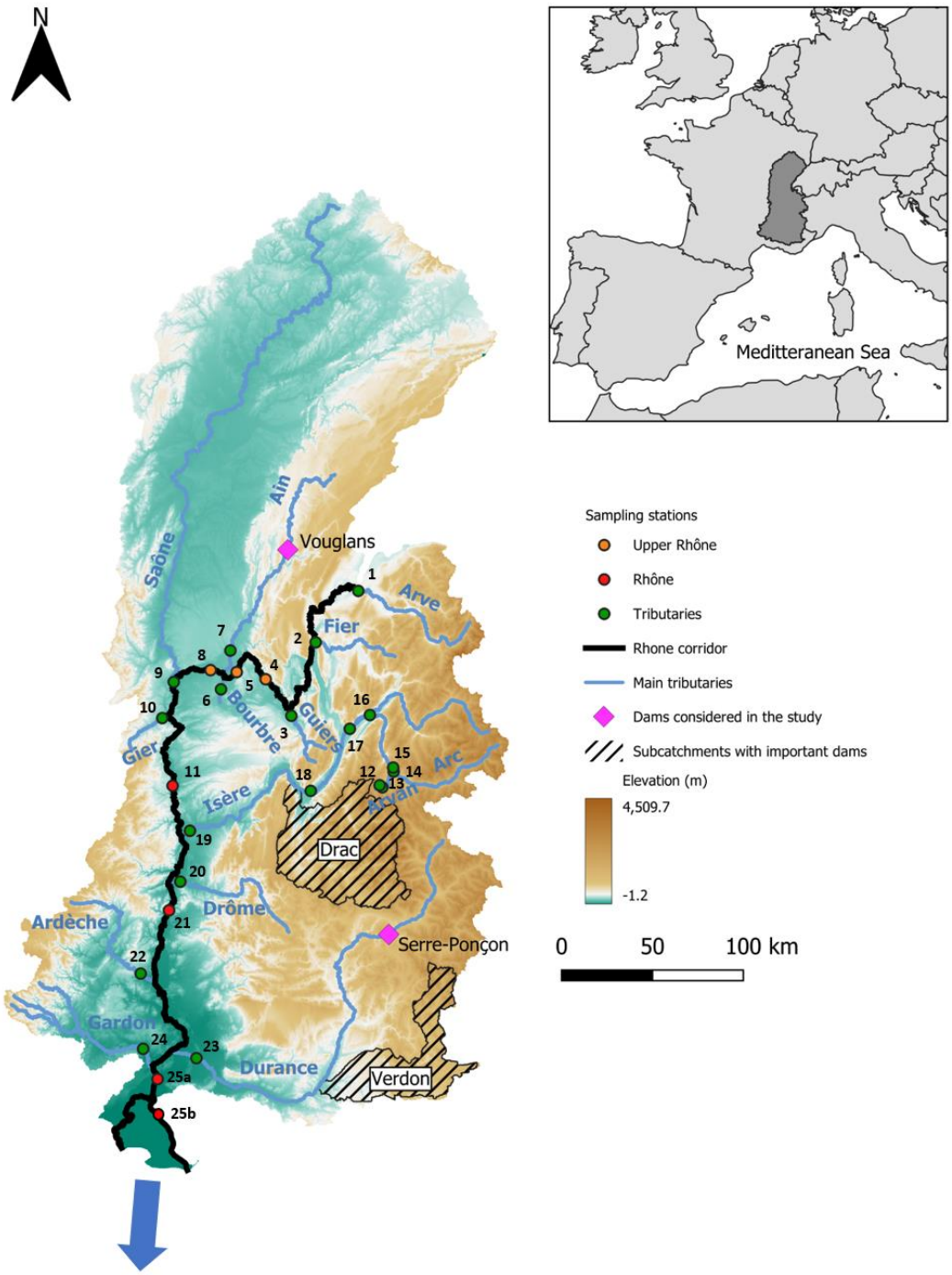

Figure 1: The river network of the Rhône River and its main tributaries. The sampling stations used in this study cover multiple parts of the mainstream and several tributaries of the Rhône catchment. Details on the stations can be found in Table 1. The arrow designates the flow direction.

Table 1: Sampling stations used in the study and corresponding streams. Locations of the stations can be found in Figure 1

Station number	Station	Stream
1	Genève	Arve
2	Motz	Fier
3	Belmont	Guiers
4	Bugey	Upper Rhône
5	Creys	Upper Rhône
6	Tignieu-Jameyzieu	Bourbre
7	Pont-de-Chazey	Ain
8	Jons	Upper Rhône
9	Lyon	Saône
10	Givors	Gier
11	Andancette	Rhône
12	Saint-Sorlin-d'Arves	Arvan
13	Villette	Arvan
14	Saint-Jean-de-Maurienne	Arvan
15	Pontamafrey	Arc
16	Chamousset	Arc
17	Montmelian	Isère
18	Grenoble	Isère
19	Beaumont-Monteux	Isère
20	Livron	Drôme
21	Cruas	Rhône
22	Saint-Martin-d'Ardèche	Ardèche
23	Bonpas	Durance
24	Remoulins	Gardon
25a	Beaucaire	Rhône
25b	Arles	Rhône

The monitoring network is based on the *Rhône Sediment Observatory* (OSR) program. It includes 25 sampling stations covering multiple catchments of various sizes (Figure 1; Table 1). The monitoring network consists of the permanent survey of water level (with regular gauging to derive flow) and turbidity (with regular samplings to derive SPM concentration and thus fluxes). More information on the monitoring network can be found in Thollet et al. (2021) and Lepage et al. (2021). Six stations are located on the Rhône corridor. The others are mainly located on the major tributaries close to the confluence with the Rhône River. The historical outlet gauging station at Beaucaire (station 25a) covers 98% of the catchment area. For SPM concentrations, measurements from the Arles station (station 25b), located 4km downstream of the Beaucaire station, were used. SPM concentrations at Beaucaire are assumed to be close to those measured at Arles. Five other stations deliver SPM concentrations at different stages of the Rhône corridor (Figure 1). Most tributaries are covered by one station at their outlet except for the Isère catchment, which presents eight stations, including those of the Arc River and the Arvan River (Thollet et al., 2021; Figure 1). Our period of study is between 2010 and 2019.

3 Materials and methods

Two models have been acquired or constructed over the study area to model fine sediment transfers. Models outputs were compared to SPM fluxes monitored in the 23 sampling stations regularly distributed over the catchment. Figure 2 presents a general flow chart of the employed methodology and main parameters used to construct the two models.

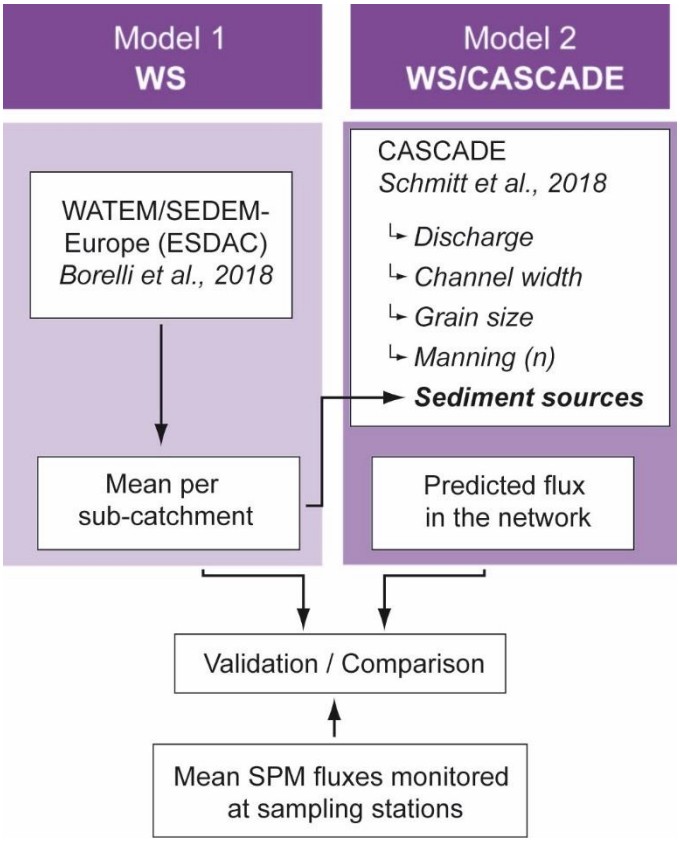

Figure 2: General flow chart of the methodology used in this study.

3.1 Soil erosion models

3.1.1 The WaTEM/SEDEM (WS) model

Borelli et al. (2018) modelled the long-term annual rates of soil loss, sediment transfer and deposition in $Mg.ha^{-1}.y^{-1}$ at the European scale using the Water and Tillage Erosion Model (WaTEM/SEDEM, Van Oost et al., 2000). WaTEM/SEDEM (WS) is an extension of the Revised Universal Soil Loss Equation (RUSLE) model from Panagos et al. (2015). Based on topography and land cover, the eroded material estimated with RUSLE by Panagos et al. (2015; Model 1) is routed to the nearest stream according to a transport capacity formula. Therefore, part of the eroded material estimated by RUSLE is deposited before reaching the nearest stream (about 85% of the total amount at the European scale). WS at the European scale was developed with a high-resolution (25 m) digital elevation model (DEM). Borelli et al.

(2018) provide more details on the model calibration. The model can be downloaded at https://esdac.jrc.ec.europa.eu/themes/sediment-transport-using-watemsedem.

3.1.2 Soil loss estimates by soil erosion models

Figure 3 details the net soil loss rates estimated by both models at the scale of the French part of the Rhône catchment. By considering deposition before entering rivers, Borelli et al. (2018) showed that only 15.3% of the total eroded soil estimated by RUSLE at the European scale is routed to the streams in WS. In the Rhône catchment, the average net soil loss estimated by is 0.98 ± 4.35 $Mg.ha^{-1}.y^{-1}$. As a comparison, RUSLE returns a sediment yield of 4.30 ± 5.96 $Mg.ha^{-1}.y^{-1}$ at the Rhône scale (Panagos et al., 2015), resulting in a Sediment Delivery Ratio of 22.8%, slightly higher than the European average. It is important to note that WS does not evaluate soil loss in areas that are not prone to soil erosion, such as urban areas, bare rocks, glaciers, wetlands, lakes, rivers, and inland waters (Borelli et al., 2018). Therefore, high-elevated areas, especially in the Alps, do not have net soil loss values.

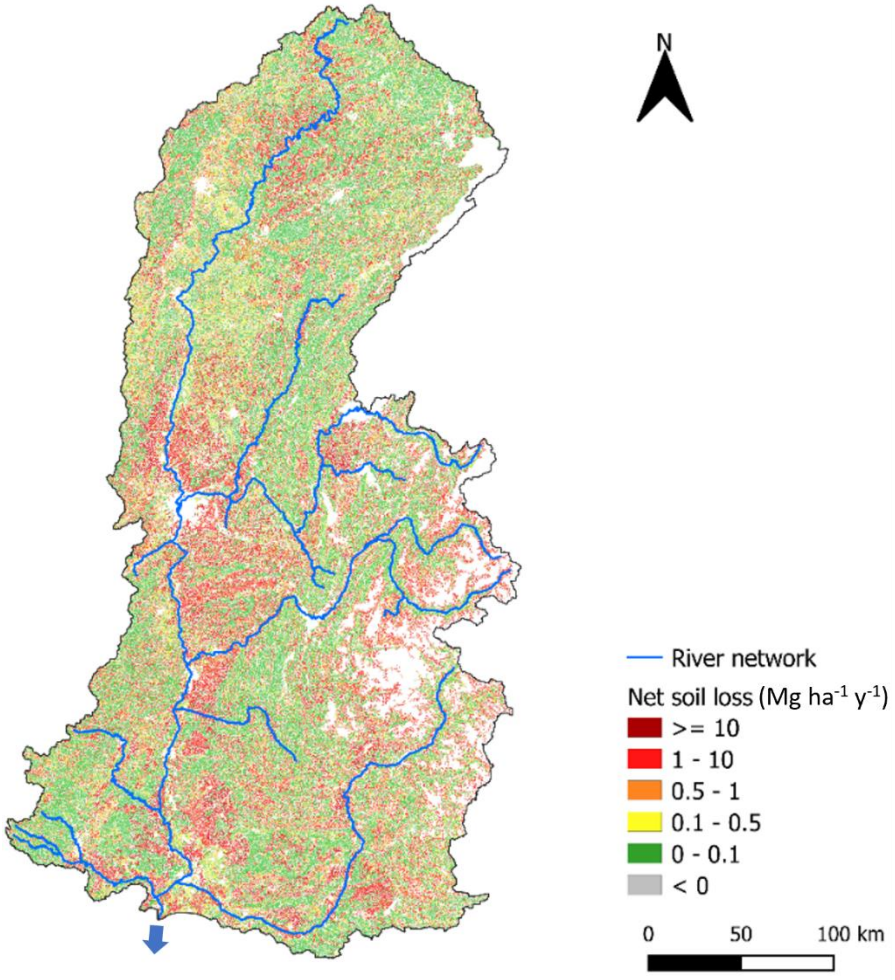

Figure 3: Net soil loss rates (in Mg ha^{-1} y^{-1}) estimated by the WaTEM/SEDEM model (25m resolution) from Borelli et al. (2018) at the Rhône scale.

3.2 Sediment connectivity tool: the CASCADE model

3.2.1 Presentation

The CAtchment Sediment Connectivity And Delivery (CASCADE) model was developed by Schmitt et al. (2016, 2018). It provides information regarding sediment connectivity at the river network scale by combining graph theory and sediment transport modelling (Tangi et al., 2019). The main advantage of CASCADE is the quantification of sediment loads with spatial information about their provenance and destination. It is achieved by simulating the fate of sediment loads and their interaction with downstream processes. CASCADE was developed to provide spatial information on sediment transport processes and the impacts of alterations in the river network, such as human infrastructures.

As inputs, CASCADE requires a river network as a succession of nodes and reaches. Hydromorphologic attributes related to sediment transport are assigned to each reach (slope, length, drained area, discharge, active channel width, grain size distribution, and Manning's roughness coefficient). These attributes are used to calculate the transport capacity of each reach, i.e. the amount of energy available to transport sediment of a specific size. The user can choose between the following four sediment transport formulas: Engelund and Hansen (1967), Wilcock and Crowe (2003), Wong and Parker (2006), and Yang (1973) and others can be implemented by the users if needed. These transport formulas mainly represent bed-material load (Church, 2006) with emphasis on bedload or suspended load according to the formula implemented.

To estimate fine sediment (< 8 mm) transport in CASCADE, several adaptations have been necessary. Indeed, CASCADE adopts common sediment transport formula developed in the literature. Sediment transport formulas tend in the vast majority to represent the bed material and not the suspended load that we are aiming in this paper. Therefore, we modified the original version of the model to set a limit of transported materials as the total fine sediment reaching the river as estimated by the WaTEM/SEDEM model.

Concerning external sources and barriers, the user can add dams that retain materials or sediment sources from the hillslopes or riverbanks.

CASCADE is a static model simulating the instantaneous sediment transport fluxes in each reach for a single discharge value. By looping over the different discharge quantiles, CASCADE can represent the dynamic of the mean hydrological cycle. Details on the functioning of CASCADE can be found on the model website (http://cascade.deib.polimi.it/) or in Tangi et al. (2019).

3.2.2 Modelling inputs

3.2.2.1 River Network

River network delineation was done using the TopoToolbox (Figure 1; Schwanghart and Scherler, 2014). TopoToolbox comprises Matlab functions that analyse relief and flow pathways in digital elevation models (DEMs). TopoToolbox can delineate river networks and calculate the terrain attributes CASCADE requires, such as slope. More information on the TopoToolbox can be found at https://topotoolbox.wordpress.com/. We used the BD Alti® as the source DEM (https://geoservices.ign.fr/bdalti) with a resolution of 25m. Pre-processing based on Wang and Liu (2006) fill sinks algorithm were performed before implementing it in CASCADE.

We selected the Rhône corridor and its main tributaries to be part of the modelled network as fine sediment is sampled at their outlets. We also added the Arc and the Arvan rivers (Figure 1) because of the high amount of monitoring data available in the Arc-Isère observatory (Thollet et al., 2021). The stream reaches were partitioned manually by using breaknodes separating reaches assumed to have different geomorphological characteristics.

3.2.2.2 Discharge

Discharge data were extracted from the distributed hydrological model J2000-Rhône (Branger et al., 2016; Morel et al., 2023). J2000-Rhône is an adaptation of the hydrologic model J2000 on the Rhône River catchment (Krause, 2001). As J2000, J2000-Rhône is based on Hydrological Response Units (HRUs). These HRUs have homogeneous landscape characteristics, such as slope, altitude, soils, or land use, and delineate areas that are assumed to be subject to similar hydrological processes. The version of J2000-Rhône from which we extracted discharge data includes multiple dams. The river network from J2000-Rhône differ from the river network delineated by TopoToolbox and used in this study. Therefore, for each stream of the river network, we manually attributed the corresponding stream in J2000-Rhône to represent the evolution of discharge along the Rhône River and its main tributaries.

Simulated yearly average discharges over the 2010-2019 period are within the range of observed values at the different monitoring sites, with a slight underestimation of 11.6% (Table 2).

To estimate annual sediment fluxes, CASCADE processes with yearly discharge quantiles. In this study, we used the following quantiles (0.1, 10, 30, 50, 70, 90, 99.9, and 100% of water discharges) to represent the different hydrologic conditions. Therefore, we calculated these quantiles for each stream of the CASCADE river network.

Table 2: Comparison of observed and simulated yearly average water discharges with J2000-Rhône at the different monitoring sites over the 2010-2019 period.

Station number	Station	Stream	Obs. ($m^3 s^{-1}$)	Sim. (J2000; $m^3 s^{-1}$)	Bias (%)
1	Genève	Arve	73.9	60.1	-18.7
2	Motz	Fier	41.2	33.7	-18.2
3	Belmont	Guiers	16.0	15.3	-4.5
4	Bugey	Upper Rhône	-	444.5	
5	Creys	Upper Rhône	457.0	438.7	-4.0
6	Tignieu-Jameyzieu	Bourbre	7.7	8.6	12.9
7	Pont-de-Chazey	Ain	123.0	95.2	-22.6
8	Jons	Upper Rhône	457.0	562.4	23.1
9	Lyon	Saône	473.0	445.8	-5.8
10	Givors	Gier	3.2	3.4	6.6
11	Andancette	Rhône	-	1046.9	
12	Saint-Sorlin-d'Arves	Arvan	1.2	1.0	-17.5
13	Villette	Arvan	1.2	1.0	-13.3
14	Saint-Jean-de-Maurienne	Arvan	2.8	2.4	-15.4
15	Pontamafrey	Arc	30.0	18.0	-40.1
16	Chamousset	Arc	49.1	56.2	14.6
17	Montmelian	Isère	121.0	99.4	-17.8
18	Grenoble	Isère	178.0	117.7	-33.9
19	Beaumont-Monteux	Isère	333.0	227.2	-31.8
20	Livron	Drôme	20.0	14.4	-28.2
21	Cruas	Rhône	-	1344.0	
22	Saint-Martin-d'Ardèche	Ardèche	65.0	58.2	-10.4
23	Bonpas	Durance	190.0	141.2	-25.7
24	Remoulins	Gardon	32.7	31.8	-2.7
25a	Beaucaire	Rhône	1690.0	1660.8	-1.7
Average					-11.6

3.2.2.3 Active flow width

Morel et al. (2019) calculated active flow widths for every stream in France, including the Rhône River. In this study, we used their formula based on the discharge as follows:

$$W_i^{(ac)} = a\, Q_i^b$$

where $W_i^{(ac)}$ is the active flow width for stream i (m), Q_i is the discharge for stream i ($m^3.s^{-1}$), a is a parameter specific to the geomorphology of the catchment, while b is linked to the riverbed characteristics, particularly the changes of active flow widths regarding discharge variations. a and b are determined for each stream based on Morel et al. (2019).

3.2.2.4 Manning-Strickler coefficients

Manning-Strickler coefficients (n) were calculated for each reach based on multiple observations available in the scientific literature and technical reports (Figure 4). Correlations were computed between n and hydromorphological parameters, such as slope, active flow

width, or average discharge in the considered streams, which are variables used to determine n (Manning et al., 1890). Each of these correlations was made independently for each stream, and the final value was selected based on the best-fitting regression analysis. For most streams, slope was found to be the best variable for predicting n, agreeing with experimental studies (Hessel et al., 2003; Marcus et al., 1992). All correlations are in Appendix 1 and some of them can be found in Figure 4 as examples.

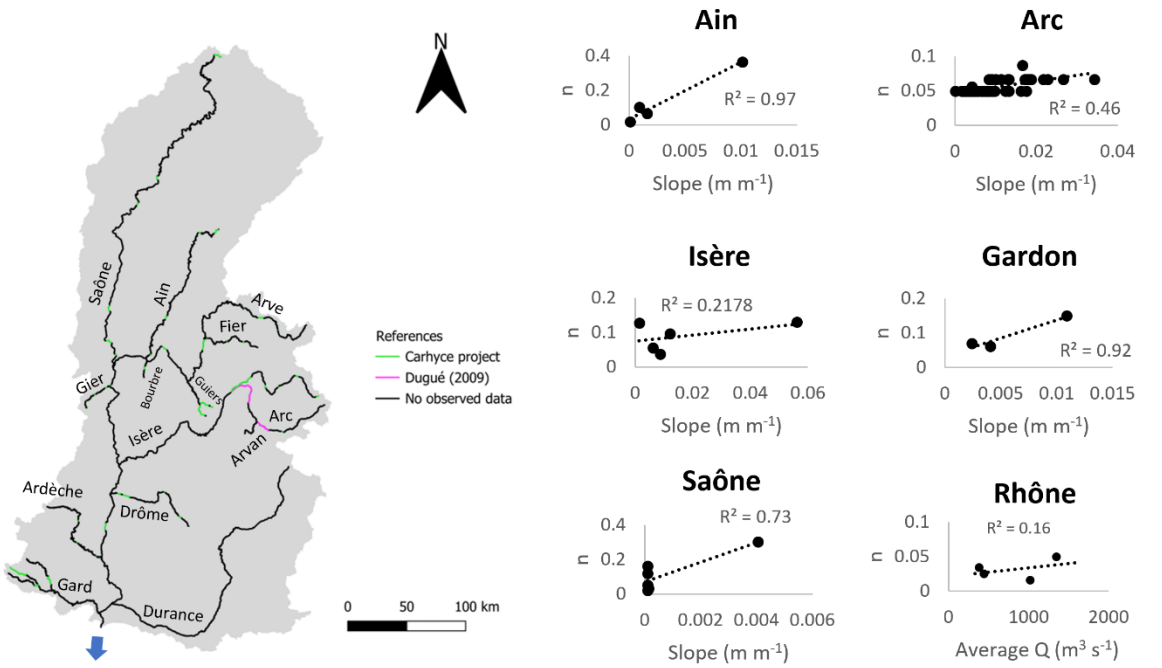

Figure 4: Manning-Strickler coefficients (n) for several tributaries and the Rhône corridor based on observations and hydromorphological parameters. Data comes from Dugué (2009) and from the CARHYCE project (https://carhyce.eaufrance.fr/). Q stands for discharge.

CASCADE needs to define the modelled sediment classes based on the Φ scale (Krumbein, 1934), which is a logarithmic scale describing grain size and computed as follows:

$$\Phi = -\log_2 \frac{D}{D_0} \quad (281)$$

where Φ is the Krumbein phi scale, D is the diameter of the particle in millimetres, and D_0 is a reference diameter, equal to 1 mm, kept to make the equation dimensionally consistent.

In this study, we intend to simulate suspended load. Usually, grains smaller than 0.125 mm tend to travel in suspension (Wilcock et al., 2009). Coarse grains (> 8 mm) tend to travel as bedload. In between, grains travel as bedload or suspended load, depending on the strength of the flow (Wilcock et al., 2009). As we chose to simulate fine sediment, we chose to simulate particles with a diameter between 0.001 and 8 mm, i.e., a φ value between -3 and 10 (Table

289 3). Part of the simulated flux might be transported by bed load, but we assume it is negligible
290 compared to the total suspended load by restricting φ values between -3 and 10.

291 *Table 3: Classification of grains in CASCADE to simulate suspended load based on Krumbein (1934).*

Classification	Φ scale	Size (mm)
Silt/Clay	4 to 10	0.001 – 0.062
Sand	-1 to 4	0.062 – 2
Gravel	-3 to -1	2 - 8

292

293 #### 3.2.2.5 Transport capacity formula

294 CASCADE integrates several transport capacity formulas adapted to each sediment
295 particle size class simulated. This paper assesses how well CASCADE can simulate fine
296 sediment transport mainly supplied by soil erosion models such as WS. We used the Yang
297 formula among the available transport capacity formulas (Yang, 1973). This formula is a total
298 load transport equation which bases transport on stream power, the product of velocity and
299 shear stress. The equation comprises two separate relations for sand and gravel transport. In
300 this study, we decided to use the relation for sand transport, as a part of the sand is transported
301 within the suspended load (Krumbein, 1934; Wilcock et al., 2009).

302 #### 3.2.2.6 Dams

303 In large watersheds such as the Rhône, dams have impacts on the water cycle and may
304 be able to trap fine sediment. Multiple dams are located on the Rhône corridor and its
305 tributaries. In this study, where we focus on fine sediment transfer at a yearly timescale, we
306 only considered the largest dams directly influencing downstream transport. On the modelled
307 network, we included two large dams (Serre-Ponçon on the Durance River and Vouglans on
308 the Ain River; Figure 1) that are known to interrupt the sediment connectivity (their trapping
309 coefficient of fine sediment in CASCADE was set to 100%). Other dams known to interrupt the
310 sediment connectivity are in the Drac and the Verdon subcatchments. They were considered
311 by not providing fine sediment sources to the streams in these two subcatchments (Figure 1).
312 Other facilities were not considered as we assume their influence on fine sediment connectivity
313 is negligible at a yearly timescale, since regular flushes (yearly in the Alps) are performed to
314 avoid sediment accumulation upstream. Only their influence on discharge was considered, as
315 they are included in J2000-Rhône.

316 #### 3.2.2.7 Suspended sediment grain size distribution and sediment sources

317 Regular grain size distribution measurements of SPM (about one sample per month) were
318 conducted at each monitoring station used in this study. They were collected in the framework
319 of the *Rhône Sediment Observatory* (OSR; http://graie.org/osr/). Locations of the
320 measurements can be found in Figure 1. Table 4 shows the average grain size distribution of

the suspended load for each sampling station. Data were not available for each tributary. For these streams, we attributed the values from the closest station downstream, e.g., the Jons station on the Rhône corridor for the Guiers, the Ain, and the Bourbre rivers.

Table 4: Average suspended sediment grain size distribution (D_{10}, D_{50}, and D_{84}) for each stream during the period of study. The closest station with grain size distribution data is selected. Values are estimated based on the Rhône Sediment Observatory and the Arc-Isère databases.

Stream (or section)	Selected station (station number)	D_{10} (mm)	D_{50} (mm)	D_{90} (mm)
Arve	Jons (8)	$3.38\ 10^{-3}$	$9.91\ 10^{-3}$	$4.57\ 10^{-2}$
Fier	Motz (2)	$2.81\ 10^{-3}$	$2.34\ 10^{-2}$	$7.30\ 10^{-2}$
Guiers	Jons (8)	$3.38\ 10^{-3}$	$9.91\ 10^{-3}$	$4.57\ 10^{-2}$
Ain	Jons (8)	$3.38\ 10^{-3}$	$9.91\ 10^{-3}$	$4.57\ 10^{-2}$
Bourbre	Jons (8)	$3.38\ 10^{-3}$	$9.91\ 10^{-3}$	$4.57\ 10^{-2}$
Saône	Lyon (9)	$2.67\ 10^{-3}$	$1.22\ 10^{-2}$	$4.34\ 10^{-2}$
Gier	Givors (10)	$6.57\ 10^{-3}$	$2.79\ 10^{-2}$	$8.52\ 10^{-2}$
Arvan	Beaumont-Monteux (19)	$4.39\ 10^{-3}$	$1.98\ 10^{-2}$	$5.49\ 10^{-2}$
Arc	Beaumont-Monteux (19)	$4.39\ 10^{-3}$	$1.98\ 10^{-2}$	$5.49\ 10^{-2}$
Isère	Beaumont-Monteux (19)	$4.39\ 10^{-3}$	$1.98\ 10^{-2}$	$5.49\ 10^{-2}$
Drôme	Livron (20)	$2.60\ 10^{-3}$	$2.08\ 10^{-2}$	$7.04\ 10^{-2}$
Ardèche	Saint-Martin-d'Ardèche (22)	$5.28\ 10^{-3}$	$2.59\ 10^{-2}$	$8.88\ 10^{-2}$
Durance	Bonpas (23)	$2.75\ 10^{-3}$	$1.79\ 10^{-2}$	$6.67\ 10^{-2}$
Gardon	Remoulins (24)	$6.07\ 10^{-3}$	$2.51\ 10^{-2}$	$7.60\ 10^{-2}$
Rhône (from Geneva Lake to Jons)	Jons (8)	$3.38\ 10^{-3}$	$9.91\ 10^{-3}$	$4.57\ 10^{-2}$
Rhône (from Jons to Andancette)	Andancette (11)	$3.17\ 10^{-3}$	$1.61\ 10^{-2}$	$5.88\ 10^{-2}$
Rhône (from Andancette to Arles)	Arles (25b)	$4.54\ 10^{-3}$	$1.97\ 10^{-2}$	$5.55\ 10^{-2}$

The transport of hillslope sediments to each stream of the river network was calculated based on the WS model (Borelli et al., 2018) described in section 3.1. This model provides long-term averages of annual soil loss and deposition rates at the European scale. For each reach in our river network, we delineated the area that drains directly to the reach and calculated the average soil loss rate in this area. Then, we attributed this value to each stream as the average soil loss rate of its drained hillslopes.

Concerning the granulometry of sources, we assumed that they are close to the values observed in the river. Therefore, we attributed to each sub-catchment the values of D10, D50 and D90 from the closest monitoring station as shown in Table 4.

4 Results

4.1 Models parameters and inputs

4.1.1 The sediment sources models and their integration into CASCADE

The aggregation of the mean erosion rates at the scale of small sub-catchments allow (1) a first description of the location of sediment sources at the catchment scale and (2) the

integration of these inputs as sediment sources in the CASCADE framework. WS provides erosion rates of 0.98 ± 4.35 $Mg.ha^{-1}.y^{-1}$ for the whole Rhône catchment, ranging from 0 to 1318.3 $Mg.ha^{-1}.y^{-1}$.

Figure 5 shows sub-catchment scale aggregated sediment transport to the river network modelled using WS. Higher erosion rates characterise the alpine region. It is particularly true regarding the central alpine massifs, including the upstream Isère, the Arc and the upstream Durance valleys. On the contrary, several alpine catchments show lower sediment transport rates, probably due to catchment connectivity properties (e.g., southeastern basins, upstream Durance). The Saône catchment (Figure 1) and most central and southern catchments show relatively low sediment transfers to rivers, mainly between 0 and 0.05 $Mg.ha^{-1}.y^{-1}$).

A comparison between these soil loss rates calculated by WS and the SPM monitored at gauging stations will be provided in section 4.3.

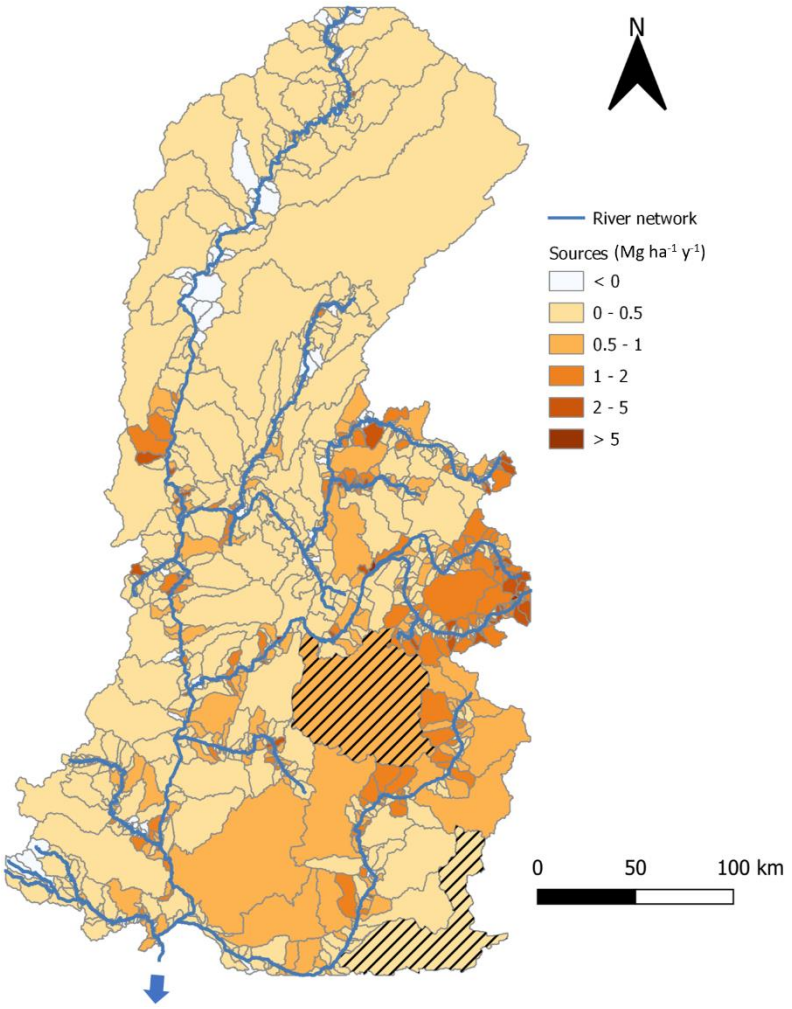

Figure 5: Estimates of net erosion with WaTEM/SEDEM in each sub-catchment. Sources from hatched subcatchments are set to 0 $Mg.ha^{-1}.y^{-1}$ due to dams influence.

4.1.2 Stream network parameters of the CASCADE model

The average values of the four main parameters enabling CASCADE to predict sediment yield are presented in Figure 6. A classical progressive discharge rise from upstream to downstream can be observed with a maximum value of 1,625 $m^3.s^{-1}$ at the catchment outlet (Figure 6a). At the regional scale, the map illustrates the significant contribution of the upstream part of the Rhône and the Saône rivers to the total discharge. Alpine catchments (i.e., Isère and Durance) also contribute significantly to the Rhône discharge. The active flow width is directly deduced from discharge and thus shows a consistent pattern at the regional scale (Figure 6b).

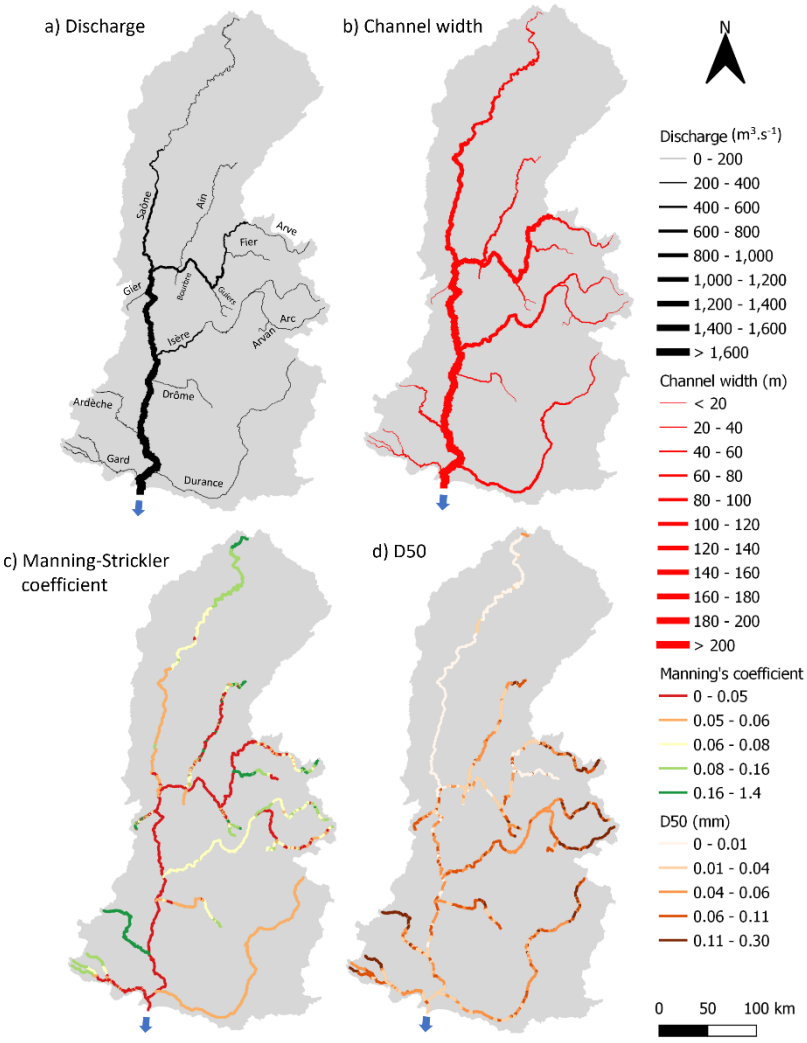

Figure 6: Details on the average values of the main CASCADE parameters (a: discharge, b: active flow width, c: Manning's coefficient, d: D50) in each stream.

The mean Manning-Strickler coefficient is 0.184 (Figure 6c). It is irregularly distributed over the catchment. The Rhône corridor is characterised by the lowest values, from 0 to 0.05.

Conversely, the highest values are located upstream of the main Alpine watersheds (i.e., the Fier and the Isère rivers), and upstream of the Saône and the Ain rivers. The Ardèche is also characterised by high Manning-Strickler coefficients. On their downstream parts, the main tributaries (Saône, Drôme, Isère, Durance) have low to average values (between 0.05 and 0.08).

Regarding grain size distribution (Figure 6d), the Saône River stands out for the low D50 values observed (i.e., between below 0.01 mm). The other tributaries and the Rhône corridor show higher values. Most of the rivers present a general pattern organised as a progressive decrease of the D50 from upstream (values above 0.11 mm) to downstream (between 0.04 and 0.06 mm).

4.2 Sediment fluxes and deposition returned by WS/CASCADE

WS/CASCADE (Model 2) shows relatively consistent patterns at the regional scale, even if absolute values differ (Figure 7).

The Isère, Saône, and Durance rivers are the main contributors to the total fine sediment fluxes (respectively 0.43, 0.50, 0.41 $Tg.y^{-1}$) and show a progressive rise from up to downstream. The upper Rhône (from Geneva Lake to Lyon) is also characterised by important sediment fluxes (0.31 $Tg.y^{-1}$ at Jons) with major contributions from the Arve (0.07 $Tg.y^{-1}$) and the Ain rivers (0.05 $Tg.y^{-1}$). The other smaller tributaries show lower contributions to total fluxes.

Very few sections show significant deposition patterns. The main deposition areas can be found directly upstream of the two main dams that were included in the models (i.e., Serre-Ponçon – Durance- and Vouglans – Ain). The lower valleys of the Ardèche River and the Fier River, characterised by large and flat floodplains, also show wide deposition patterns directly linked to the shallow slopes of these reaches.

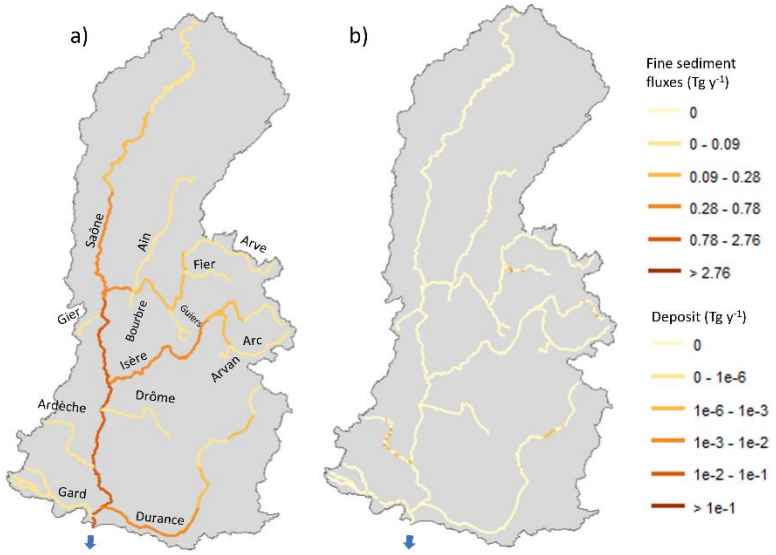

Figure 7: Transported (a) and deposited (b) fine sediment in Tg y^{-1} evaluated in Model 2 in each reach.

4.3 Comparison between models and validation

Figure 8 compares the modelled fine sediment fluxes using the two models tested in this paper with the mean interannual fluxes monitored at the 25 sampling stations. Both models are well correlated with observed fluxes with Pearson correlation coefficients above 0.85, returning slight underestimations for most of the monitoring sites. Model 1 slightly underestimates the exports (-34.9% on average; Appendix 2).

By considering Model 1 as sediment sources for CASCADE, the resulting estimates are decreasing, indicating the occurrence of significant sediment deposition potential in the river network (-51.7% on average with Model 2).

Following these results, Model 1 provides the best fitting with the observed values. In contrast, Model 2 provides relatively satisfying results that remain within the order of magnitude of the observed data, even if it underestimates sediment fluxes.

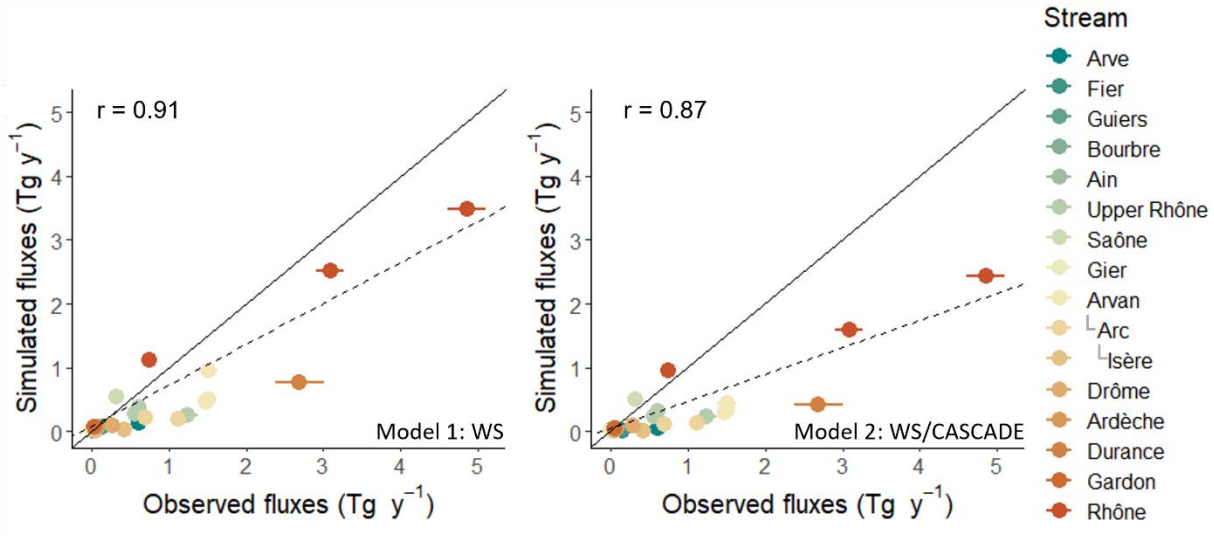

Figure 8: Comparison between observed and simulated fluxes for Model 1 (left) and Model 2 (right). Fluxes simulated by Model 1 are soil loss rates considering that all sediment entering the stream cannot deposit while fluxes simulated by Model 2 are in-stream fluxes. The legend is ordered based on the tributaries entering the Rhône corridor from upstream to downstream.

Figure 9 shows the deviation between observed and simulated fluxes at each monitoring site. It highlights the general underestimation of Models 1 and 2. For Model 1, exports from eastern streams coming from the Alps (mainly the Arve, the Isère, and the Durance rivers) present the largest underestimations. Concerning Model 2, few exports are well predicted (Appendix 2), such as the Bourbre River (+8.1%), the Gardon River (-4.6%), or the Guiers River (-19.8%). Others are overestimated, like the Gier River (+78.0%) or the Saône River (+53.1%). The exports from the remaining rivers are underestimated. By focusing on the most significant fluxes, the deviation at the Rhône outlet is mainly due to an underestimation of the Durance export that propagates downstream.

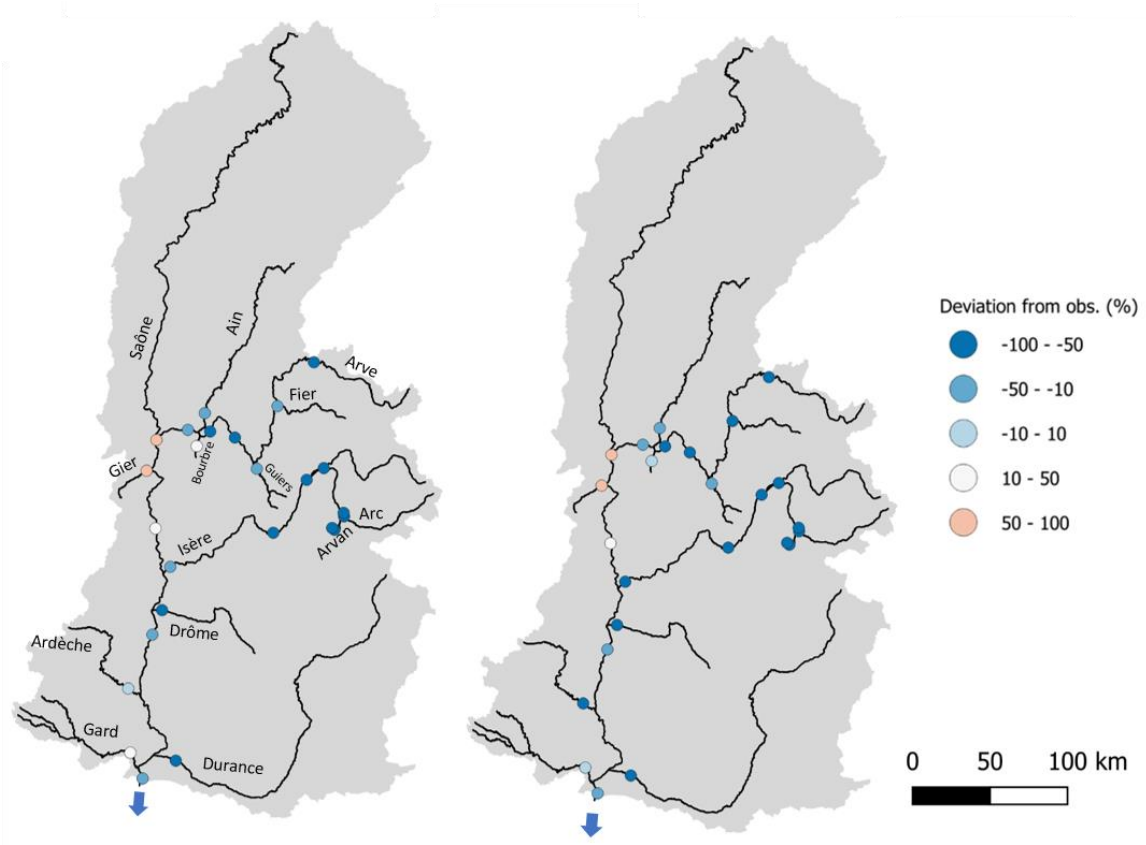

Figure 9: Relative differences between observed and simulated fluxes at each monitoring station with WS (left) and WS/CASCADE (right). Fluxes simulated WS are soil loss rates considering that all sediment entering the stream cannot deposit while fluxes simulated by WS/CASCADE are in-stream fluxes. Details on the values can be found in Appendix 2.

4.4 In-stream deposition and sediment connectivity of the main tributaries to the Rhône corridor

Table 5 details the amount of deposited materials estimated by Model 2 in each sub-catchment. It shows that most of the deposition occurs in the Durance River (58.4%), especially in the Serre-Ponçon dam, one of the most important dams in the Rhône catchment, followed by the Fier (16.4%) and the Ardèche (13.5%) rivers. At the sub-catchment scale, most of the materials entering the stream in the Ardèche and the Fier deposits before being exported (59.0% and 80.1%, respectively). This can be explained by the shallow slopes in the downstream alluvial plains. The Ain and the Durance rivers are also poorly connected since about 30% of the flux is retained, mainly in dams.

Table 5: Estimates of deposition and connectivity in each sub-catchment with WS/CASCADE. The connectivity is estimated by comparing the flux at the outlet to the total amount of sediment entering the stream.

Stream	Deposition				Connectivity		
	Deposited material ($Tg.y^{-1}$)	% of deposit in dams	% of deposit compared to flux simulated at monitoring site	% of the total deposit in the whole catchment	Flux exported ($Tg.y^{-1}$)	Sources ($Tg.y^{-1}$)	Connectivity (%)
Ain	$2.0\ 10^{-2}$	99.9	30.5	6.2	$4.5\ 10^{-2}$	$6.5\ 10^{-2}$	69.6
Arc	$1.0\ 10^{-6}$	-	$7.5\ 10^{-4}$	$3.1\ 10^{-4}$	$1.3\ 10^{-1}$	$1.3\ 10^{-1}$	100
Ardèche	$4.3\ 10^{-2}$	-	59.0	13.5	$3.0\ 10^{-2}$	7.3 10-2	41.0
Arvan	0	-	0	0	$1.5\ 10^{-2}$	$1.5\ 10^{-2}$	99.9
Arve	0	-	0	0	$6.8\ 10^{-2}$	$6.8\ 10^{-2}$	100
Bourbre	0	-	0	0	$2.6\ 10^{-2}$	$2.6\ 10^{-2}$	100
Drôme	$3.2\ 10^{-3}$	-	4.0	1.0	$7.7\ 10^{-2}$	$8.0\ 10^{-2}$	96.9
Durance	$1.9\ 10^{-1}$	99.9	31.2	58.4	$4.1\ 10^{-1}$	$6.0\ 10^{-1}$	68.9
Fier	$5.2\ 10^{-2}$	-	80.1	16.4	$1.3\ 10^{-2}$	$6.5\ 10^{-2}$	19.9
Gardon	$1.6\ 10^{-3}$	-	2.9	0.5	$5.5\ 10^{-2}$	$5.7\ 10^{-2}$	97.2
Gier	$1.4\ 10^{-5}$	-	0.1	$6.0\ 10^{-3}$	$2.3\ 10^{-2}$	$2.3\ 10^{-2}$	100
Guiers	0	-	0	0	$1.1\ 10^{-2}$	$1.2\ 10^{-2}$	94.0
Isère	$1.2\ 10^{-2}$	-	2.8	3.9	$4.3\ 10^{-1}$	$4.4\ 10^{-1}$	97.1
Rhône	0	-	0	0	$2.4\ 10^{-1}$	$2.9\ 10^{-1}$	84.1
Saône	$1.0\ 10^{-6}$	-	$2.0\ 10^{-4}$	$3.0\ 10^{-4}$	$5.0\ 10^{-1}$	$5.0\ 10^{-1}$	100

By comparing the flux estimated at each monitoring site to the total amount of sediment entering the stream in the corresponding drained catchment, we could assess the suspended load connectivity of each tributary to the Rhône River.

The Ain and the Durance rivers are 69.6% and 68.9% connected (meaning that 69.6% and 68.9% of the sediment that reaches the stream in the catchment will effectively enter the Rhône corridor at a one-year timescale period). These values are mainly due to the presence of large dams that interrupt the sediment connectivity (Citterio and Piegay, 2009; Rollet et al., 2014), which is highlighted in Table 5 and Appendix 2. Only two catchments present low to very low connectivity values (i.e. the Fier with 19.9% and the Ardèche with 41.0%) mainly due to deposits occurring close to the confluence (Figure 7 & Table 5). The remaining catchments present high connectivity (above 90%) as they present no or few deposits, and no large dams retain the suspended load.

By comparing the results obtained with WS alone and with WS coupled with CASCADE, we can approach the role of the river in transporting materials in a large catchment (Table 6). Coupling WS with CASCADE reduces the exported fluxes ranging from 5.4% to 83.3% (according to the tributary).

Table 6: Simulated suspended load differences between Models 1 (WS) and 2 (WS/CASCADE).

Stream	Model 1 ($Tg.y^{-1}$)	Model 2 ($Tg.y^{-1}$)	Difference (%)
Ain	0.07	0.04	-35.3
Arc	0.20	0.13	-35.5
Ardèche	0.07	0.02	-68.5
Arvan	0.02	0.02	-12.7
Arve	0.13	0.06	-57.3
Bourbre	0.03	0.02	-15.5
Drôme	0.08	0.08	-6.0
Durance	0.77	0.41	-46.8
Fier	0.08	0.01	-83.3
Gardon	0.06	0.04	-24.5
Gier	0.02	0.01	-5.4
Guiers	0.01	0.01	-9.2
Isère	0.95	0.43	-54.8
Rhône	3.48	2.43	-30.0
Saône	0.53	0.49	-6.7
Upper Rhône	0.25	0.22	-11.1

5 Discussion

5.1 Sediment connectivity and erosion models

This paper intends to evaluate the abilities of WS coupled or not with the CASCADE toolbox to represent suspended load in a large catchment. From a fundamental point of view, hillslope erosion models alone underestimate the effects of the stream on sediment dynamics in a watershed as they consider that sediment entering the stream proceeds automatically to the outlet (Hamel et al., 2015; Van Rompaey et al., 2001). Indeed, in-stream processes or obstacles within the stream, such as large dams, may alter or improve sediment connectivity (Czuba and Foufoula-Georgiou, 2015; Schmitt et al., 2018). The CASCADE toolbox fills this gap and coupling it with soil erosion models may represent actual sediment dynamics in a large watershed (Tangi et al., 2019).

Indeed, comparing WS estimates with in-stream concentrations is inadequate but coupling them with CASCADE helps in considering riverine processes, which may reproduce observed dynamics. Here, we showed that WS is a good input for CASCADE as the coupling returns simulations close to actual sources delivered to the streams in the Rhône catchment.

Nevertheless, both approaches with WS underestimated the exported fluxes but returned results close to the observations. WS is a European-scale model and may not be adapted at a catchment scale. A soil erosion model adapted to the Rhône catchment may be developed and tested to pass through this issue. The ideal answer that may be obtained with the latter may be between slightly higher than WS estimations.

From a fundamental point of view, RUSLE-derived models as WS strictly represent the rill and inter-rill erosion processes (Renard et al., 1997), which are often the main processes involved in most agricultural lands and hilly valleys in the catchment. However, the erosion

493 dynamics in the mountains are more complex and involve a wide variety of processes, such
494 as gully erosion, debris flow, or landslides, which are known to contribute significantly to the
495 transfer of sediments to rivers (Cossart et al., 2018; Remaître et al., 2005; Theule et al., 2012).
496 As mentioned in the introduction, these processes are more difficult to model (especially
497 regarding volumes contribution to rivers), and their integration into the CASCADE framework
498 remains challenging, especially at such a large scale. In the case of the Rhône catchment, a
499 potential solution might be to apply correction factors to sediment sources depending on their
500 susceptibility to mass movement processes.

501 In this study, we used the Yang (1973) formula to model SPM transfers in the network,
502 which accounts for different ranges of particle sizes depending on transport capacity of flow
503 (Table 3). This formula was not developed for suspended load simulations. This may be a main
504 source of uncertainty as our validation data are suspended load data. Therefore, completing
505 our observed data with bed material fluxes may help in using CASCADE at the scale of the
506 Rhône.

507 RUSLE-based models generally account for particles below 1 mm (Renard et al., 1997;
508 Vigiak et al., 2012). The SPM monitoring using water flow meters coupled with turbidity sensors
509 may measure various grain size ranges but generally below 0.125 mm (Wilcock et al., 2009).
510 In that sense, it is generally considered that turbidity sensors are very sensitive to grain size
511 and that the suspended sand fraction might be greatly underestimated (e.g., Foster et al., 1992;
512 Camenen et al., 2018; 2020). Thus, it can be assumed that most of the observed fluxes coming
513 from monitoring stations, especially for catchments draining the Alps, might underestimate the
514 sand fraction transported in the suspended load. This consideration must be accounted when
515 comparing measured and modelled values. More generally, the variety of the considered grain
516 size distributions simplified under the term of SPM may lead to imprecision in both the
517 modelling framework and the comparison of models with SPM monitoring values for validation.

518 ### 5.2 Potential methodological and dataset improvements

519 In this section, we tried to explain the deviation we obtained between the observed and the
520 simulated fluxes estimated with Models 1 and 2. These deviations may come from different
521 steps of the modelling process. First, we tried to estimate the missing information in the
522 sediment inputs from hillslopes. As shown in Figure 2, WS estimates do not cover the entire
523 Rhône catchment. Indeed, soil loss rates are not estimated by this model in high-elevated
524 areas due to the presence of glaciers or bare rocks. Nevertheless, we assume that these areas
525 might play a non-negligible role in bringing materials to the streams. Part of the
526 underestimations in our study might be explained by this missing information. To highlight this
527 link, we calculated for each monitoring site the coverage of the erosion model and the average

elevation in its total catchment area and compared those values to the deviations (Figure 10). We found that sub-catchments with underestimated fluxes are mainly sub-catchments where the WS raster only covers between 50 and 80% of the total catchment area. In the same way, these sub-catchments have a high mean elevation, meaning that mountainous sub-catchments appear to be the main areas where underestimation is observable. Correcting this deviation in the estimates of sediment sources might improve our simulations at the different outlets.

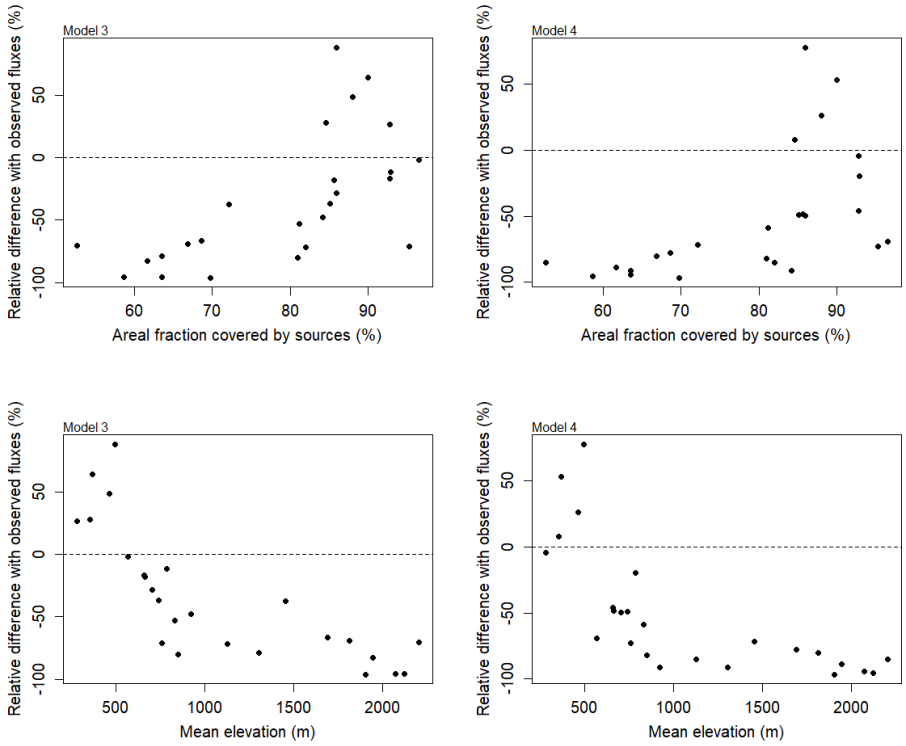

Figure 10: Relative differences and differences between observed fluxes and simulations with WS and with CASCADE compared with the areal fraction covered by external sources and the mean elevation in each sub-catchment.

Second, simulated water exports at the monitoring sites show deviations between -40.1% and +14.6%, where most sites have underestimated exports (Table 2). Indeed, Figure 11 shows that most of the sites with an underestimated flux in fine sediment also have low discharge values compared to observations. The discharge representation may then explain a part of the underestimation of sediment fluxes by coupling WS with CASCADE. Nevertheless, some sites present higher discharge values while sediment fluxes are still underestimated.

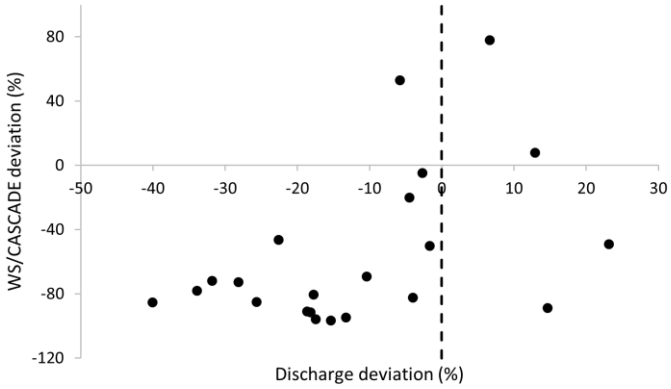

546

547 *Figure 11: Comparison between deviations in discharge and fine sediment fluxes. The x axis corresponds to*
548 *deviations between observed discharges and those simulated by J2000-Rhône. The y axis shows the deviations*
549 *between observed fine sediment fluxes and those simulated by Model 2.*

550

551 It is important to note that the river networks delineated in J2000-Rhône and CASCADE
552 differ. Discharge values for each reach of the CASCADE's river network were chosen by
553 manually selecting the closest reach in the J2000-Rhône's channels, which could lead to
554 misestimations in discharge in some reaches.

555 We used a simplified version of the stream network, only considering the main tributaries
556 to the Rhône River, i.e. where fine sediment is sampled. This is also due to the limited
557 hydrological and geomorphological information available in other smaller rivers in the Rhône
558 catchment. However, the numerous small tributaries may collectively have a significant
559 influence at the catchment scale, which cannot be evaluated yet. This study uses the static
560 version of CASCADE to estimate the average annual export in the Rhône River based on
561 discharge quantiles. This approach does not represent flash floods occurring in some sub-
562 catchments or any flushing of the dams in the whole catchment. Using the recently developed
563 dynamic version of CASCADE (D-CASCADE; Tangi et al., 2022) may help capture the
564 temporal variability occurring in the Rhône catchment. Nevertheless, the complexity of this
565 watershed, highly influenced by anthropogenic activities, may be hard to capture in a dynamic
566 approach.

567 This study considered only two dams known to interrupt the sediment connectivity (Figure
568 1). Some other dams were considered by not considering sources coming from their respective
569 subcatchments (Figure 5). However, multiple dams are implemented on the Rhône River and
570 its main tributaries. Even if these dams do not stop the sediment connectivity, they may slow
571 down the exported fluxes or retain a substantial part of the suspended loads. As the Rhône
572 catchment counts about 50 dams and multiple weirs, even if local retention is low, the total

amount of materials retained may not be negligible, especially for the largest materials (e.g., Belletti et al., 2020).

5.3 Sediment sources compared with other local studies

We assessed the origin of the suspended load at Beaucaire (the outlet) and at Jons, the sampling station draining the Upper Rhône catchment (Figure 12), as previous research explored SPM origins in these two stations using tracers or fingerprinting. We showed that most of the suspended load comes from the Rhône corridor. At Jons, the main tributaries feeding the Rhône load are the Arve, the Ain, and the Bourbre rivers. Dabrin et al. (2021) also found a main contribution of the Arve to the suspended load at Jons by using a 1-D hydro-sedimentary model and a fingerprinting approach. Dabrin et al. (2021) also observed a substantial contribution from the Fier River, which we do not find with our approach. Indeed, we observe important deposition in some sections of the Fier (Figure 7). An inadequate parameterisation of these sections, such as a bad representation of slopes or Manning-Strickler coefficients, might explain the important deposition. Thus, we might underestimate the actual contribution of this tributary to the total fluxes.

At the Rhône outlet, the main contributors are the Saône, the Durance, and the Isère. Here, using tracers, Bégorre et al. (2022) reconstructed the contributions of the main tributaries to the Rhône River outlet from 1980 to 2015. In the last decade, they found a significant contribution from the Durance watershed, followed by the Ardèche and the Isère catchments. In the same way, observed fluxes show that the Durance and the Isère rivers deliver to the Rhône corridor about half of the suspended load observed at the outlet (Poulier et al., 2019). The Durance River may play a more important role than what is presented in Figure 10 because CASCADE largely underestimates the exports (-84.8%) on this tributary, probably due to both discharge and sediment sources underestimations as mentioned in sections 4.4 and 5.2. Indeed, simulated discharge at the outlet of the Durance is 25% lower than observations. Concerning sediment sources, the erosion map covers a limited fraction of the Durance catchment (82%). This excludes noteworthy mountain areas very sensitive to erosion and sediment transfers which might be important sources of sediments to the Durance (e.g., the marly Badlands of the Alpine foothills, Ariango et al., 2021; Klotz et al., 2023).

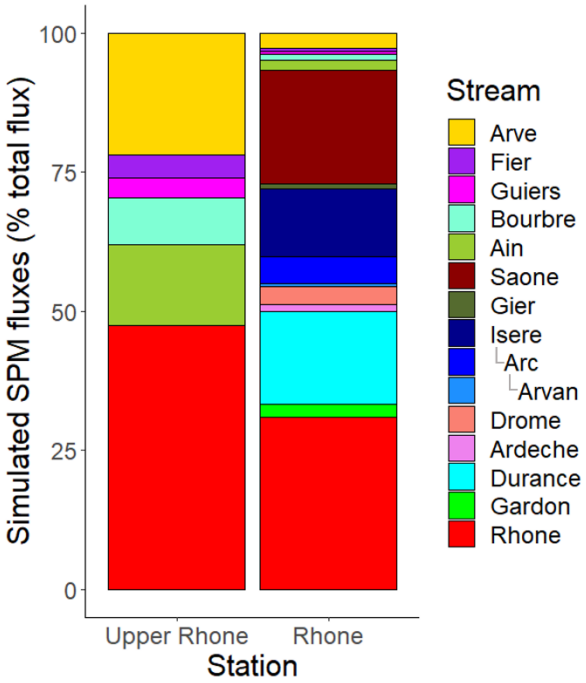

603

604 *Figure 12: Origin of suspended load in the Upper Rhône at Jons (left) and at the outlet of the Rhône at Beaucaire*
605 *(right).*

606

607 ## 6 Conclusion

608 This work attempted to show the role of in-stream connectivity models such as CASCADE
609 in representing fine sediment dynamics in a large basin with numerous anthropogenic
610 disturbances, such as the Rhône. Nevertheless, the coupling of CASCADE with
611 WaTEM/SEDEM returned fluxes further from observations than WaTEM/SEDEM alone. These
612 deviations may come from many sources, e.g. discharge data, misestimates of erosion in high-
613 elevated areas, unadapted transport capacity formulas, or unadapted validation data.

614 Future applications should generate better data in terms of amount and size of sources
615 supply for the missing zones neglected by traditional soil erosion models (e.g., landslides,
616 mountain areas) to further explore the added value of coupling CASCADE with a soil erosion
617 model. As well as better representation of dam trapping efficiencies and hydrological
618 simulations could further enhance our ability to predict fine sediment dynamics at large scale
619 and highlight the significance and necessity of a proper representation of river network
620 connectivity. Increasing our monitoring assets across the basin to include all processes
621 involved with fine sediment generation will provide the ability to have plausible ranges of
622 sediment supply and then to develop integrated (soil erosion, detachment processes, river
623 network connectivity) models capable to provide robust fine sediment predictions in the near
624 future.

7 References

Alewell, C., Borrelli, P., Meusburger, K., Panagos, P., 2019. Using the USLE: Chances, challenges and limitations of soil erosion modelling. International soil and water conservation research 7, 203–225.

Ariagno, C., Le Bouteiller, C., Van Der Beek, P., Klotz, S., 2022. Sediment export in marly badland catchments modulated by frost-cracking intensity, Draix–Bléone Critical Zone Observatory, SE France. Earth Surf. Dynam. 10, 81–96. https://doi.org/10.5194/esurf-10-81-2022

Baartman, J.E.M., Temme, A.J.A.M., Saco, P.M., 2018. The effect of landform variation on vegetation patterning and related sediment dynamics. Earth Surf Processes Landf 43, 2121–2135. https://doi.org/10.1002/esp.4377

Bégorre, C., Dabrin, A., Masson, M., Mourier, B., Eyrolle, F., Lepage, H., Morereau, A., Coquery, M., 2022. Reconstruction of historical suspended particulate matter contributions of Rhône River tributaries to the Mediterranean Sea. Geomorphology 417, 108445.

Belletti, B., Garcia De Leaniz, C., Jones, J., Bizzi, S., Börger, L., Segura, G., Castelletti, A., Van De Bund, W., Aarestrup, K., Barry, J., Belka, K., Berkhuysen, A., Birnie-Gauvin, K., Bussettini, M., Carolli, M., Consuegra, S., Dopico, E., Feierfeil, T., Fernández, S., Fernandez Garrido, P., Garcia-Vazquez, E., Garrido, S., Giannico, G., Gough, P., Jepsen, N., Jones, P.E., Kemp, P., Kerr, J., King, J., Łapińska, M., Lázaro, G., Lucas, M.C., Marcello, L., Martin, P., McGinnity, P., O'Hanley, J., Olivo Del Amo, R., Parasiewicz, P., Pusch, M., Rincon, G., Rodriguez, C., Royte, J., Schneider, C.T., Tummers, J.S., Vallesi, S., Vowles, A., Verspoor, E., Wanningen, H., Wantzen, K.M., Wildman, L., Zalewski, M., 2020. More than one million barriers fragment Europe's rivers. Nature 588, 436–441. https://doi.org/10.1038/s41586-020-3005-2

Bizzi, S., Tangi, M., Schmitt, R.J.P., Pitlick, J., Piégay, H., Castelletti, A.F., 2021. Sediment transport at the network scale and its link to channel morphology in the braided Vjosa River system. Earth Surf Processes Landf 46, 2946–2962. https://doi.org/10.1002/esp.5225

Borrelli, P., Van Oost, K., Meusburger, K., Alewell, C., Lugato, E., Panagos, P., 2018. A step towards a holistic assessment of soil degradation in Europe: Coupling on-site erosion with sediment transfer and carbon fluxes. Environmental Research 161, 291–298. https://doi.org/10.1016/j.envres.2017.11.009

Branger, F., Gouttevin, I., Tilmant, F., Cipriani, T., Barachet, C., Montginoul, M., Le Gros, C., Sauquet, E., Braud, I., Leblois, E., 2016. Modélisation hydrologique distribuée du Rhône (Research Report). irstea.

Brierley, G., Tunnicliffe, J., Bizzi, S., Lee, F., Perry, G., Poeppl, R., Fryirs, K., 2022. Quantifying Sediment (Dis)Connectivity in the Modeling of River Systems, in: Treatise on Geomorphology. Elsevier, pp. 206–224. https://doi.org/10.1016/B978-0-12-818234-5.00161-9

Brown, C.B., 1943. Discussion of “Sedimentation in reservoirs” 69.

Brune, G.M., 1953. Trap efficiency of reservoirs. Trans. AGU 34, 407. https://doi.org/10.1029/TR034i003p00407

Camenen, B., Dramais, G., Buffet, A., Thollet, F., Le Bescond, C., Lagouy, M., Berni, C., Le Coz, J., 2018. Estimation of sand suspension in a secondary channel of an alpine river, in: E3S Web of Conferences. EDP Sciences, p. 04014.

Camenen, B., Thollet, F., Buffet, A., Dramais, G., Valette, E., Zanker, S., 2020. An estimation of the sand suspension in alpine rivers during a dam flushing event, in: River Flow 2020 (Proceedings of the 10th Conference on Fluvial Hydraulics).

Cavalli, M., Trevisani, S., Comiti, F., Marchi, L., 2013. Geomorphometric assessment of spatial sediment connectivity in small Alpine catchments. Geomorphology 188, 31–41. https://doi.org/10.1016/j.geomorph.2012.05.007

Church, M., 2006. Bed material transport and the morphology of alluvial river channels. Annu. Rev. Earth Planet. Sci. 34, 325–354. https://doi.org/10.1146/annurev.earth.33.092203.122721

Citterio, A., Piégay, H., 2009. Overbank sedimentation rates in former channel lakes: characterization and control factors. Sedimentology 56, 461–482. https://doi.org/10.1111/j.1365-3091.2008.00979.x

Cossart, É., Fressard, M., 2017. Assessment of structural sediment connectivity within catchments: insights from graph theory. Earth Surf. Dynam. 5, 253–268. https://doi.org/10.5194/esurf-5-253-2017

Cossart, E., Viel, V., Lissak, C., Reulier, R., Fressard, M., Delahaye, D., 2018. How might sediment connectivity change in space and time? Land Degrad Dev 29, 2595–2613. https://doi.org/10.1002/ldr.3022

687 Czuba, J.A., Foufoula-Georgiou, E., 2015. Dynamic connectivity in a fluvial network for
688 identifying hotspots of geomorphic change. Water Resources Research 51, 1401–1421.
689 https://doi.org/10.1002/2014WR016139

690 Dabrin, A., Bégorre, C., Bretier, M., Dugué, V., Masson, M., Le Bescond, C., Le Coz, J.,
691 Coquery, M., 2021. Reactivity of particulate element concentrations: apportionment
692 assessment of suspended particulate matter sources in the Upper Rhône River, France. J
693 Soils Sediments 21, 1256–1274. https://doi.org/10.1007/s11368-020-02856-0

694 Downs, P.W., Piégay, H., 2019. Catchment-scale cumulative impact of human activities on
695 river channels in the late Anthropocene: implications, limitations, prospect. Geomorphology
696 338, 88–104. https://doi.org/10.1016/j.geomorph.2019.03.021

697 Engelund, F., Hansen, E., 1967. A monograph on sediment transport in alluvial streams.
698 Technical University of Denmark 0stervoldgade 10, Copenhagen K.

699 Foster, I.D.L., Millington, R., Grew, R.G., 1992. The impact of particle size controls on stream
700 turbidity measurement; some implications for suspended sediment yield estimation.
701 Erosion and sediment transport monitoring programmes in river basins 210, 51–62.

702 Fressard, M., Cossart, E., 2019. A graph theory tool for assessing structural sediment
703 connectivity: Development and application in the Mercurey vineyards (France). Science of
704 The Total Environment 651, 2566–2584. https://doi.org/10.1016/j.scitotenv.2018.10.158

705 Fryirs, K.A., Brierley, G.J., Preston, N.J., Kasai, M., 2007. Buffers, barriers and blankets: The
706 (dis) connectivity of catchment-scale sediment cascades. Catena 70, 49–67.

707 Hamel, P., Chaplin-Kramer, R., Sim, S., Mueller, C., 2015. A new approach to modeling the
708 sediment retention service (InVEST 3.0): Case study of the Cape Fear catchment, North
709 Carolina, USA. Science of The Total Environment 524–525, 166–177.
710 https://doi.org/10.1016/j.scitotenv.2015.04.027

711 Hamel, P., Falinski, K., Sharp, R., Auerbach, D.A., Sánchez-Canales, M., Dennedy-Frank,
712 P.J., 2017. Sediment delivery modeling in practice: Comparing the effects of watershed
713 characteristics and data resolution across hydroclimatic regions. Science of the Total
714 Environment 580, 1381–1388.

715 Heckmann, T., Cavalli, M., Cerdan, O., Foerster, S., Javaux, M., Lode, E., Smetanová, A.,
716 Vericat, D., Brardinoni, F., 2018. Indices of sediment connectivity: opportunities,
717 challenges and limitations. Earth-Science Reviews 187, 77–108.
718 https://doi.org/10.1016/j.earscirev.2018.08.004

Heckmann, T., Schwanghart, W., 2013. Geomorphic coupling and sediment connectivity in an alpine catchment — Exploring sediment cascades using graph theory. Geomorphology 182, 89–103. https://doi.org/10.1016/j.geomorph.2012.10.033

Heckmann, T., Schwanghart, W., Phillips, J.D., 2015. Graph theory—Recent developments of its application in geomorphology. Geomorphology 243, 130–146. https://doi.org/10.1016/j.geomorph.2014.12.024

Hessel, R., Jetten, V., Guanghui, Z., 2003. Estimating Manning's n for steep slopes. CATENA 54, 77–91. https://doi.org/10.1016/S0341-8162(03)00058-4

Hirschberg, J., Fatichi, S., Bennett, G.L., McArdell, B.W., Peleg, N., Lane, S.N., Schlunegger, F., Molnar, P., 2021. Climate Change Impacts on Sediment Yield and Debris-Flow Activity in an Alpine Catchment. JGR Earth Surface 126, e2020JF005739. https://doi.org/10.1029/2020JF005739

Hooftman, D., Bullock, J., Evans, P., Redhead, J., Ridding, L., Varma, V., Pywell, R., 2023. A model of sediment retention by vegetation for Great Britain: new methodologies & validation. bioRxiv 2023.08. 17.553678.

Khan, S., Fryirs, K., Bizzi, S., 2021. Modelling sediment (dis)connectivity across a river network to understand locational-transmission-filter sensitivity for identifying hotspots of potential geomorphic adjustment. Earth Surf Processes Landf 46, 2856–2869. https://doi.org/10.1002/esp.5213

Klotz, S., Le Bouteiller, C., Mathys, N., Fontaine, F., Ravanat, X., Olivier, J.-E., Liébault, F., Jantzi, H., Coulmeau, P., Richard, D., Cambon, J.-P., Meunier, M., 2023. A high-frequency, long-term data set of hydrology and sediment yield: the alpine badland catchments of Draix-Bléone Observatory. Earth Syst. Sci. Data 15, 4371–4388. https://doi.org/10.5194/essd-15-4371-2023

Kondolf, G.M., 1997. PROFILE: Hungry Water: Effects of Dams and Gravel Mining on River Channels. Environmental Management 21, 533–551. https://doi.org/10.1007/s002679900048

Kondolf, G.M., Rubin, Z.K., Minear, J.T., 2014. Dams on the Mekong: Cumulative sediment starvation. Water Resources Research 50, 5158–5169.

Kondolf, G.M., Schmitt, R.J., Carling, P., Darby, S., Arias, M., Bizzi, S., Castelletti, A., Cochrane, T.A., Gibson, S., Kummu, M., 2018. Changing sediment budget of the Mekong: Cumulative threats and management strategies for a large river basin. Science of the total environment 625, 114–134.

Kondolf, G.M., Schmitt, R.J.P., Carling, P.A., Goichot, M., Keskinen, M., Arias, M.E., Bizzi, S., Castelletti, A., Cochrane, T.A., Darby, S.E., Kummu, M., Minderhoud, P.S.J., Nguyen, D., Nguyen, H.T., Nguyen, N.T., Oeurng, C., Opperman, J., Rubin, Z., San, D.C., Schmeier, S., Wild, T., 2022. Save the Mekong Delta from drowning. Science 376, 583–585. https://doi.org/10.1126/science.abm5176

Krause, P., 2001. Das hydrologische Modellsystem J2000: Beschreibung und Anwendung in grossen Flussgebieten, Schriften des Forschungszentrums Jülich. Forschungszentrum, Zentralbibliothek, Jülich.

Krumbein, W.C., 1934. Size Frequency Distributions of Sediments. SEPM JSR Vol. 4. https://doi.org/10.1306/D4268EB9-2B26-11D7-8648000102C1865D

Lepage, H., Gruat, A., Thollet, F., Le Coz, J., Coquery, M., Masson, M., Dabrin, A., Radakovitch, O., Eyrolle, F., Labille, J., Jean-Paul, A., Delanghe, D., Raimbault, P., 2021. Concentrations and fluxes of suspended particulate matters and associated contaminants in the Rhône River from Lake Geneva to the Mediterranean Sea. https://doi.org/10.15454/RJCQZ7

Manning, R., Griffith, J.P., Pigot, T.F., Vernon-Harcourt, L.F., 1890. On the flow of water in open channels and pipes.

Marcus, W.A., Roberts, K., Harvey, L., Tackman, G., 1992. An evaluation of methods for estimating Manning's n in small mountain streams. Mountain Research and Development 227–239.

Morel, M., Pella, H., Branger, F., Sauquet, E., Grenouillet, G., Côte, J., Braud, I., Lamouroux, N., 2023. Catchment-scale applications of hydraulic habitat models: Climate change effects on fish. Ecohydrology 16, e2513. https://doi.org/10.1002/eco.2513

Morel, M., Tamisier, V., Pella, H., Booker, D.J., Navratil, O., Piégay, H., Gob, F., Lamouroux, N., 2019. Revisiting the drivers of at-a-station hydraulic geometry in stream reaches. Geomorphology 328, 44–56. https://doi.org/10.1016/j.geomorph.2018.12.007

Najafi, S., Dragovich, D., Heckmann, T., Sadeghi, S.H., 2021. Sediment connectivity concepts and approaches. Catena 196, 104880.

Panagos, P., Borrelli, P., Poesen, J., Ballabio, C., Lugato, E., Meusburger, K., Montanarella, L., Alewell, C., 2015. The new assessment of soil loss by water erosion in Europe. Environmental Science & Policy 54, 438–447. https://doi.org/10.1016/j.envsci.2015.08.012

Paquier, A., 1999. Etude hydraulique de l'Arc de Maurienne (de Modane à l'Isère) - Synthèse.

784 Posner, S., Verutes, G., Koh, I., Denu, D., Ricketts, T., 2016. Global use of ecosystem service
785 models. Ecosystem Services 17, 131–141.

786 Poulier, G., Launay, M., Le Bescond, C., Thollet, F., Coquery, M., Le Coz, J., 2019. Combining
787 flux monitoring and data reconstruction to establish annual budgets of suspended
788 particulate matter, mercury and PCB in the Rhône River from Lake Geneva to the
789 Mediterranean Sea. Science of The Total Environment 658, 457–473.
790 https://doi.org/10.1016/j.scitotenv.2018.12.075

791 Recking, A., 2017. Elements de géomorphologie fluviale. Cahier 2 : La granulométrie des cours
792 d'eau (et sa mesure). Irstea.

793 Recking, A., 2013. An analysis of nonlinearity effects on bed load transport prediction:
794 Nonlinearity and bed load prediction. J. Geophys. Res. Earth Surf. 118, 1264–1281.
795 https://doi.org/10.1002/jgrf.20090

796 Remaître, A., Malet, J.-P., Maquaire, O., 2005. Morphology and sedimentology of a complex
797 debris flow in a clay-shale basin: Morphology and sedimentology of a debris flow. Earth
798 Surf. Process. Landforms 30, 339–348. https://doi.org/10.1002/esp.1161

799 Renard, K.G., USA, USA (Eds.), 1997. Predicting soil erosion by water: a guide to conservation
800 planning with the revised universal soil loss equation (RUSLE), Agriculture handbook.
801 Washington, D. C.

802 Richter, B.D., Postel, S., Revenga, C., Scudder, T., Lehner, B., Churchill, A., Chow, M., 2010.
803 Lost in development's shadow: The downstream human consequences of dams. Water
804 alternatives 3, 14.

805 Rollet, A.J., Piégay, H., Dufour, S., Bornette, G., Persat, H., 2014. Assessment of
806 consequences of sediment deficit on a gravel river bed downstream of dams in restoration
807 perspectives: application of a multicriteria, hierarchical and spatially explicit diagnosis:
808 sediment deficit consequences. River Res. Applic. 30, 939–953.
809 https://doi.org/10.1002/rra.2689

810 Rossi, L.M.W., Rapidel, B., Roupsard, O., Villatoro-sánchez, M., Mao, Z., Nespoulous, J.,
811 Perez, J., Prieto, I., Roumet, C., Metselaar, K., Schoorl, J.M., Claessens, L., Stokes, A.,
812 2017. Sensitivity of the landslide model LAPSUS_LS to vegetation and soil parameters.
813 Ecological Engineering 109, 249–255. https://doi.org/10.1016/j.ecoleng.2017.08.010

814 Schmitt, R.J., Bizzi, S., Castelletti, A., 2016. Tracking multiple sediment cascades at the river
815 network scale identifies controls and emerging patterns of sediment connectivity. Water
816 Resources Research 52, 3941–3965.

817 Schmitt, R.J.P., Bizzi, S., Castelletti, A.F., Kondolf, G.M., 2018. Stochastic Modeling of
818 Sediment Connectivity for Reconstructing Sand Fluxes and Origins in the Unmonitored Se
819 Kong, Se San, and Sre Pok Tributaries of the Mekong River. JGR Earth Surface 123, 2–
820 25. https://doi.org/10.1002/2016JF004105

821 Schwanghart, W., Scherler, D., 2014. Short Communication: TopoToolbox 2 – MATLAB-based
822 software for topographic analysis and modeling in Earth surface sciences. Earth Surf.
823 Dynam. 2, 1–7. https://doi.org/10.5194/esurf-2-1-2014

824 Siyam, A.M., Mirghani, M., El zein, S., Golla, S., El-sayed, S.M., 2005. Assessment of the
825 Current State of the Nile basin Reservoir Sedimentation problems. NBCN-RE (Nile Basin
826 Capacity Building Network for River Engineering), River Morphology, Research Cluster,
827 Group–I Report.

828 Syvitski, J., Ángel, J.R., Saito, Y., Overeem, I., Vörösmarty, C.J., Wang, H., Olago, D., 2022.
829 Earth's sediment cycle during the Anthropocene. Nature Reviews Earth & Environment 3,
830 179–196.

831 Syvitski, J.P., Kettner, A.J., Overeem, I., Hutton, E.W., Hannon, M.T., Brakenridge, G.R., Day,
832 J., Vörösmarty, C., Saito, Y., Giosan, L., 2009. Sinking deltas due to human activities.
833 Nature Geoscience 2, 681–686.

834 Tan, G., Chen, P., Deng, J., Xu, Q., Tang, R., Feng, Z., Yi, R., 2019. Review and improvement
835 of conventional models for reservoir sediment trapping efficiency. Heliyon 5, e02458.
836 https://doi.org/10.1016/j.heliyon.2019.e02458

837 Tangi, M., Bizzi, S., Fryirs, K., Castelletti, A., 2022. A Dynamic, Network Scale Sediment
838 (Dis)Connectivity Model to Reconstruct Historical Sediment Transfer and River Reach
839 Sediment Budgets. Water Resources Research 58, e2021WR030784.
840 https://doi.org/10.1029/2021WR030784

841 Tangi, M., Schmitt, R., Bizzi, S., Castelletti, A., 2019. The CASCADE toolbox for analyzing
842 river sediment connectivity and management. Environmental Modelling & Software 119,
843 400–406.

844 Theule, J.I., Liébault, F., Loye, A., Laigle, D., Jaboyedoff, M., 2012. Sediment budget
845 monitoring of debris-flow and bedload transport in the Manival Torrent, SE France. Nat.
846 Hazards Earth Syst. Sci. 12, 731–749. https://doi.org/10.5194/nhess-12-731-2012

847 Thollet, F., Le Bescond, C., Lagouy, M., Gruat, A., Grisot, G., Le Coz, J., Coquery, M., Lepage,
848 H., Gairoard, S., Gattacceca, J.C., Ambrosi, J.-P., Radakovitch, O., Dur, G., Richard, L.,

Giner, F., Eyrolle, F., Angot, H., Mourier, D., Bonnefoy, A., Dugué, V., Launay, M., Troudet, L., Labille, J., Kieffer, L., 2021. Observatoire des Sédiments du Rhône, INRAE.

Van Oost, K., Govers, G., Desmet, P., 2000. Evaluating the effects of changes in landscape structure on soil erosion by water and tillage. Landscape ecology 15, 577–589.

Van Rompaey, A., Bazzoffi, P., Jones, R.J., Montanarella, L., 2005. Modeling sediment yields in Italian catchments. Geomorphology 65, 157–169.

Van Rompaey, A.J.J., Verstraeten, G., Van Oost, K., Govers, G., Poesen, J., 2001. Modelling mean annual sediment yield using a distributed approach. Earth Surf. Process. Landforms 26, 1221–1236. https://doi.org/10.1002/esp.275

Vigiak, O., Borselli, L., Newham, L.T.H., McInnes, J., Roberts, A.M., 2012. Comparison of conceptual landscape metrics to define hillslope-scale sediment delivery ratio. Geomorphology 138, 74–88. https://doi.org/10.1016/j.geomorph.2011.08.026

Vörösmarty, C.J., Meybeck, M., Fekete, B., Sharma, K., Green, P., Syvitski, J.P., 2003. Anthropogenic sediment retention: major global impact from registered river impoundments. Global and planetary change 39, 169–190.

Wang, L., Liu, H., 2006. An efficient method for identifying and filling surface depressions in digital elevation models for hydrologic analysis and modelling. International Journal of Geographical Information Science 20, 193–213. https://doi.org/10.1080/13658810500433453

Wilcock, P.R., Crowe, J.C., 2003. Surface-based Transport Model for Mixed-Size Sediment. J. Hydraul. Eng. 129, 120–128. https://doi.org/10.1061/(ASCE)0733-9429(2003)129:2(120)

Wilcock, P.R., Pitlick, J., Cui, Y., 2009. Sediment transport primer: estimating bed-material transport in gravel-bed rivers. US Department of Agriculture, Forest Service, Rocky Mountain Research.

Wong, M., Parker, G., 2006. Reanalysis and Correction of Bed-Load Relation of Meyer-Peter and Müller Using Their Own Database. J. Hydraul. Eng. 132, 1159–1168. https://doi.org/10.1061/(ASCE)0733-9429(2006)132:11(1159)

Yang, C.T., 1973. Incipient Motion and Sediment Transport. J. Hydr. Div. 99, 1679–1704. https://doi.org/10.1061/JYCEAJ.0003766

Zarfl, C., Dunn, F.E., 2022. The delicate balance of river sediments. Science 376, 1385–1386.